Measurement of the Michel parameters and the average τ neutrino helicity from τ decays in e$^+$e$^-$ $\rightarrow$ $\tau^+\tau^-$

The L3 Collaboration

Abstract

The Michel parameters ρ, η, ξ and $\xi\delta$, the chirality parameter ξ_h and the τ polarization $\mathcal{P}_\tau$ are measured using 32012 τ pair decays. Their values are extracted from the energy spectra of leptons and hadrons in $\tau^- \rightarrow l^- \bar{\nu}_l \nu_\tau$ and $\tau^- \rightarrow \pi^- \nu_\tau$ decays, the energy and decay angular distributions in $\tau^- \rightarrow \rho^- \nu_\tau$ decays, and the correlations in the energy spectra and angular distributions of the decay products.

Assuming universality in leptonic and semileptonic τ decays, the results are $\rho = 0.794 \pm 0.039 \pm 0.031$, $\eta = 0.25 \pm 0.17 \pm 0.11$, $\xi = 0.94 \pm 0.21 \pm 0.07$, $\xi\delta = 0.81 \pm 0.14 \pm 0.06$, $\xi_h = -0.970 \pm 0.053 \pm 0.011$, and $\mathcal{P}_\tau = -0.154 \pm 0.018 \pm 0.012$. The measurement is in agreement with the V$-$A hypothesis for the weak charged current.

Introduction

The subject of this paper is an investigation of the Lorentz structure of the charged current in leptonic and semileptonic τ decays. The undetected neutrinos and the unmeasured polarization of the outgoing lepton allow the measurement of only four Michel parameters [1] in the leptonic τ decays, $\tau^- \to l^- \bar{\nu}_l \nu_\tau$[1] ($l = $ e, μ). Of these four parameters, ρ and η describe the isotropic part of the lepton energy spectrum, while ξ and $\xi\delta$ describe the angular distribution asymmetry of the spectrum with respect to the τ spin direction. In semileptonic τ decays, $\tau^- \to h^- \nu_\tau$ ($h = \pi, K$ or ρ) [2] the chirality parameter ξ_h is interpreted as twice the average τ neutrino helicity.

In muon decays the Lorentz structure was studied with high precision supporting the Standard Model V$-$A choice of the charged current structure and placing stringent bounds on charged current interactions other than V$-$A [2,3]. The purely leptonic decays of the τ lepton allow an independent study of the structure of the charged current. The larger mass of the τ expands the range of momentum transfers from that examined in muon decay, allowing more sensitive probes for new physics whose couplings are proportional to the lepton mass.

Measurements of Michel parameters in τ lepton decays have been performed at low energy machines [4,5] and at LEP [6]. The advantage at LEP is the non-vanishing τ polarization which facilitates the measurement of ξ and $\xi\delta$.

In this analysis data collected with the L3 detector in 1991, 1992 and 1993 are used. The Michel parameters ρ, η, ξ and $\xi\delta$, the chirality parameter ξ_h and the average τ polarization $\mathcal{P}_\tau$ are determined from a combined fit to the energy spectra of leptons and hadrons from $\tau^- \to l^- \bar{\nu}_l \nu_\tau$ and $\tau^- \to \pi^- \nu_\tau$ decays, energy and decay angular distributions in $\tau^- \to \rho^- \nu_\tau$ decays, and the correlations in the joint distributions of the decay products of both τ's.

Method of the Measurement

Purely leptonic decays $\tau^- \to l^- \bar{\nu}_l \nu_\tau$ can be described by the most general four-fermion contact interaction Hamiltonian [1]. The matrix element in the helicity projection form can be written as [7,8]:

$$\mathcal{M} = \frac{4G_F}{\sqrt{2}} \sum_{\substack{\gamma = S, V, T \\ \lambda, \iota = R, L}} g_{\lambda\iota}^\gamma < \bar{l}_\lambda |\Gamma^\gamma|(\nu_l)_n > < (\bar{\nu}_\tau)_m |\Gamma_\gamma|\tau_\iota > . \tag{1}$$

Here G_F is the Fermi constant, γ labels the scalar, vector and tensor interactions and λ, ι the chiral projections of the charged leptons. The neutrino helicities, n and m, are fixed when γ, λ and ι are given. The 10 complex coupling constants $g_{\lambda\iota}^\gamma$ can be expressed in terms of Michel parameters [8]. Four of them, ρ, η, ξ and $\xi\delta$, appear together with the average τ polarization $\mathcal{P}_\tau$ in the charged lepton decay spectrum of the τ [9]:

$$
\begin{aligned}
\frac{1}{\Gamma}\frac{d\Gamma(\tau^- \to l^- \nu_l \nu_\tau)}{dx_l} &= h_0^l(x_l) + \eta h_\eta^l(x_l) + \rho h_\rho^l(x_l) - \mathcal{P}_\tau \left[\xi h_\xi^l(x_l) + \xi\delta h_{\xi\delta}^l(x_l)\right] \\
&= \mathrm{H}_0^l(x_l) - \mathcal{P}_\tau \, \mathrm{H}_1^l(x_l),
\end{aligned}
\tag{2}
$$

---

[1] Formulae are given for the decay of the τ^-. In the analysis the charge conjugate decays are also used.

[2] No distinction between charged pions and kaons is made in $\tau^- \to h^- \nu_\tau$ decay.

2

where $x_l = E_l/E_\tau \approx E_l/E_{beam}$ is the normalized lepton energy in the laboratory system. The $h_i^l(x_l)$ are kinematical functions. In a similar way the semileptonic τ decays can be described with a matrix element ansatz leading to the relation [9]:

$$\frac{1}{\Gamma}\frac{d\Gamma(\tau^- \to h^-\nu_\tau)}{dx_h} = h_0^h(x_h) - \mathcal{P}_\tau \, \xi_h h_1^h(x_h) \quad = \quad \mathrm{H}_0^h(x_h) - \mathcal{P}_\tau \, \mathrm{H}_1^h(x_h), \tag{3}$$

where ξ_h is the chirality parameter for a particular decay. For $\tau^- \to \pi^-\nu_\tau$, $x_\pi = E_\pi/E_\tau \approx E_\pi/E_{beam}$ is the normalized pion energy. In the case of $\tau^- \to \rho^-\nu_\tau$, a quantity ω_ρ [10] is introduced and h_0^ρ and h_1^ρ are functions of ω_ρ. The quantity ω_ρ depends on the $\pi^\pm$ and π^0 energies and opening angle in the decay $\rho^\pm \to \pi^\pm\pi^0$ and conserves their sensitivity to the τ polarization. Qualitatively, negative values of ω_ρ are enriched by left handed τ^- and positive by right handed τ^-. In the neutral current decay $Z \to \tau^+\tau^-$, the helicities of the τ's are nearly 100% anti-correlated. The joint decay distribution for $e^+e^- \to \tau^+\tau^- \to A^\pm B^\mp n\nu$ $(n = 2,3,4)$, where A and B are e, μ, π or ρ, is [9]:

$$\frac{1}{\Gamma}\frac{d^2\Gamma}{dx_A dx_B} = \mathrm{H}_0^{(A)}(x_A)\mathrm{H}_0^{(B)}(x_B) + \mathrm{H}_1^{(A)}(x_A)\mathrm{H}_1^{(B)}(x_B) \tag{4}$$
$$- \mathcal{P}_\tau \left[\mathrm{H}_1^{(A)}(x_A)\mathrm{H}_0^{(B)}(x_B) + \mathrm{H}_0^{(A)}(x_A)\mathrm{H}_1^{(B)}(x_B)\right].$$

From this distribution, we can disentangle the Michel parameters, the chirality parameter and the average τ polarization up to a sign ambiguity. The latter is resolved taking into account the left-right asymmetry measurement from the SLD experiment [11] or the direct measurement of ξ_h in the $\tau^- \to a_1^-\nu_\tau$ decay [12].

The L3 Detector

The L3 detector is described in detail in Ref. [13]. The central tracker consists of a time expansion chamber (TEC) surrounded by two thin proportional (Z-)chambers. The TEC delivers a precise track measurement in the bending plane perpendicular to the beam direction and the Z-chambers provide a coordinate along the beam direction. The central tracker is surrounded by a fine grained and high resolution electromagnetic calorimeter (BGO) composed of Bismuth Germanium Oxide crystals, a ring of scintillation counters, a uranium and brass hadron calorimeter with proportional wire chambers readout (HCAL) and a precise muon spectrometer consisting of three layers of multiwire drift chambers.

These subdetectors are installed in a 12 m diameter solenoidal magnet which provides a uniform field of 0.5 T along the beam direction. In the following analysis only the barrel part of the detector with $|\cos\theta| < 0.7$ is used, where θ is the polar angle with respect to the electron beam direction.

The TEC transverse momentum resolution is parametrized as $\sigma_{p_T}/p_T = 0.018p_T(\mathrm{GeV}/c)$, the BGO resolution is less than 2% above 1 GeV, the HCAL energy resolution for $\pi^\pm$ is determined to be $\Delta\mathrm{E}/\mathrm{E} = 55\%/\sqrt{E}(\mathrm{GeV})+8\%$ and the transverse momentum resolution of the muon spectrometer is 2.8% for charged particles with $p_T = 45$ GeV.

Data Analysis

A data sample corresponding to a total integrated luminosity of 69 pb^{-1} collected by the L3 experiment during the 1991, 1992 and 1993 data taking periods is used in this analysis. A clean

sample of lepton pairs produced in Z decays is obtained by following the preselection described in Ref. [14]. Only low multiplicity events with a 'back–to–back' topology are accepted. Each event is divided into two hemispheres by a plane perpendicular to the thrust axis. Particles are identified independently in each hemisphere.

Lepton identification

Electron candidates consist of an energy deposition in the BGO which is electromagnetic in shape and consistent in position and energy with a track in the central tracker. The energy deposition in the HCAL must be consistent with the tail of an electromagnetic shower and be less than 3 GeV. Muon candidates consist of tracks in the muon spectrometer originating from the interaction point with a minimum ionizing particle response in BGO and HCAL. Only muons with track segments in three planes of the muon spectrometer are accepted. Muons with energies below 2.5 GeV are stopped in the calorimeter. The electron and muon identification efficiency is estimated from Monte Carlo. The average values are 84% and 65%, respectively.

Hadron identification

The selection of $\tau^- \to \pi^- \nu_\tau$ and $\tau^- \to \rho^- \nu_\tau$ uses the central tracker and the calorimeters. An algorithm [14] is applied to disentangle overlapping neutral electromagnetic clusters in the vicinity of the impact point of the charged hadron in the BGO. Around the impact point, which is precisely predicted by the central tracker, a hadronic shower whose shape is assumed energy independent is subtracted from the energy deposition. Remaining local maxima of energy deposition are subject to electromagnetic neutral cluster criteria. For accepted electromagnetic neutral clusters, the energies and angles are determined. Two distinct neutral clusters form a π^0 candidate if their invariant mass is within 40 MeV of the π^0 mass. A single neutral cluster forms a π^0 candidate if its energy exceeds 1 GeV. Its transverse energy profile has to be consistent with either a single electromagnetic shower or a two photon hypothesis for which the invariant mass is within 50 MeV of the π^0 mass. The calorimetrical energy of the hadron, consisting of the sum of the hadronic energy depositions in the BGO and the HCAL, is then combined with the measurement of the momentum in the central tracker by maximizing the likelihood for these two measurements to originate from a single hadron.

The $\tau^- \to \pi^- \nu_\tau$ selection admits no π^0 candidates and no neutral clusters with energy greater than 0.5 GeV. The energy deposition in the BGO and HCAL must be consistent with the measured track momentum.

To select $\tau^- \to \rho^- \nu_\tau$ decays, exactly one π^0 candidate is required in the hemisphere. The invariant mass of the $(\pi^- \pi^0)$ system must be in the range 0.45 to 1.20 GeV and its energy must be larger than 5 GeV. The efficiencies to identify $\tau^- \to \pi^- \nu_\tau$ and $\tau^- \to \rho^- \nu_\tau$ decays are determined from Monte Carlo to be 68% and 62%, respectively.

Event selection and background rejection

Only events with at least one identified τ decay are retained and classified into the following exclusive groups: ee, eμ, eπ, eρ, eX, $\mu\pi$, $\mu\rho$, μX, $\pi\pi$, $\pi\rho$, πX, $\rho\rho$ and ρX, where X stands for an unidentified τ decay. The fraction of misidentified τ decays in each channel is determined using a sample of simulated $e^+e^- \to \tau^+\tau^-$ events which is ten times larger than the data sample.

The final state where both τ's decay into a muon is not used due to high background from $Z \to \mu^+\mu^-(\gamma)$. Remaining non-τ background is further reduced by applying correlated cuts in both hemispheres for events classified as ee, eμ, eπ, eρ, $\mu\pi$, $\mu\rho$, $\pi\pi$, $\pi\rho$ and $\rho\rho$ decays. Bhabha and dimuon final states are rejected by requiring the total energy $E_{tot} < 0.8\sqrt{s}$. An acollinearity cut $\epsilon < 20^0$ suppresses two photon background and radiative Bhabha events. Cosmic muons are rejected by the requirement that tracks originate from the interaction point and that scintillator hits associated with a muon track are within 2 ns of the beam crossing time.

For events classified as eX and μX, the unidentified hemisphere must not be consistent with an electron and muon, respectively. The unidentified hemisphere in πX and ρX events must not be consistent with a high energy electron or muon. Bhabha, dimuon and two photon background shapes are estimated from Monte Carlo. The number of measured Bhabha, dimuon and two photon events is used for the normalization of the background. Finally, a data sample of 33763 events is selected.

Fit Procedure

We measure ρ, η, ξ, $\xi\delta$, ξ_h and $\mathcal{P}_\tau$ using a binned maximum likelihood fit to the one-dimensional energy spectra of eX, μX, πX and ρX and to the joint decay distributions of ee, eμ, eπ, eρ, $\mu\pi$, $\mu\rho$, $\pi\pi$, $\pi\rho$ and $\rho\rho$ final states. The likelihood function $\mathcal{L}$ is:

$$\mathcal{L} = \prod_{i,j} \frac{w_{ij}^{n_{ij}} e^{-w_{ij}}}{n_{ij}!},$$

where i runs over the particle spectra and j runs over the bins of each distribution in the fit. The quantity n_{ij} is the number of data events observed in bin j of the i-th decay mode and $w_{ij}(\rho, \eta, \xi, \xi\delta, \xi_h, \mathcal{P}_\tau)$ is the expected number of signal and background events. The sum $\sum_j w_{ij}$ is normalized to the total number of observed events in the corresponding distribution.

The expected number of events, w_{ij}, is obtained from the following procedure. The functions h_0^l, h_ρ^l, h_η^l, h_ξ^l, $h_{\xi\delta}^l$, h_0^h and h_1^h of Eqns.(2) and (3) are obtained from the KORALZ Monte Carlo program [15] with a modified version of the τ decay library TAUOLA [16]. For each leptonic decay channel, samples of events corresponding to different values of Michel parameters are generated. The h functions are constructed from linear combinations of the decay spectra of these samples. Initial and final state QED radiative corrections in $e^+e^- \to \tau^+\tau^-(\gamma)$, radiation in the decays $\tau^- \to l^-\bar{\nu}_l\nu_\tau$, and effects of the lepton masses are included. As an illustration, the shape of the functions $h_0^\mu, h_\rho^\mu, h_\eta^\mu, h_\xi^\mu$ and $h_{\xi\delta}^\mu$ are shown in Fig. 1 for the $\tau^- \to \mu^-\bar{\nu}_\mu\nu_\tau$ decay compared to the Born approximation [17]. As can be seen, radiative corrections distort the spectra very little. The functions for the $\tau^- \to e^-\bar{\nu}_e\nu_\tau$ decay are very similar, but the function h_η^e contains a suppression factor m_e/m_τ, so that for $\tau^- \to e^-\bar{\nu}_e\nu_\tau$ the sensitivity to η is strongly reduced. For the $\tau^- \to h^-\nu_\tau$ decays, h_0^h and h_1^h, shown in Fig. 2, are obtained in a similar way. Using the functions constructed above, the decay distributions given in Eqns. (2), (3) and (4) are convoluted with the L3 detector resolution functions $\mathcal{R}_A(x_A|\zeta)$, where x_A and ζ denote the reconstructed and true values of the variables, respectively. The electron and muon energy measurement is described by analytical resolution functions of the BGO and the muon spectrometer, which are adjusted using $Z \to e^+e^-(\gamma)$ and $Z \to \mu^+\mu^-(\gamma)$ data. The pion energy resolution was modeled by a weighted combination of the measurements from the central tracker and the calorimeters. The shape of the h_i^l functions is nearly unchanged by this procedure. The $\tau^- \to \pi^-\nu_\tau$ functions h_0^π and h_1^π are shown in Fig. 2 before and after applying the detector

resolution and acceptance correction. For the $\tau^- \to \rho^- \nu_\tau$ decay the functions h_0^ρ and h_1^ρ are obtained from a Monte Carlo sample, which is passed through the full detector simulation, reconstruction and identification procedure. In Fig. 2 these functions are compared to the generated ones.

The final signal distributions, $S_A(x_A, \alpha)$ are:

$$S_A(x_A, \alpha) = \mathcal{A}_A(x_A) \int \mathcal{R}_A(x_A|\zeta) \frac{1}{\Gamma} \frac{d\Gamma(\tau^- \to A^- n\nu)}{d\zeta} d\zeta, \qquad (5)$$

where α denotes the parameters of the fit: $\alpha = (\mathcal{P}_\tau, \rho, \eta, \xi, \xi\delta, \xi_h)$. The acceptance functions $\mathcal{A}_A(x_A)$ are determined for each decay channel A from Monte Carlo. They are flat functions of x_A except for very low energies [18].

The expectation value in a bin j is the sum of the integral of the signal $S_A(x_A, \alpha)$ over the bin and the background b_{Aj} in the same bin:

$$w_{Aj}(\alpha) = \int_{bin\ j} S_A(x_A, \alpha)\ dx + b_{Aj}. \qquad (6)$$

Two dimensional distributions are treated in the same way taking into account hemisphere correlations of the variables.

The fit is performed in a range of variables which depends on the particular final state excluding regions of vanishing acceptance. The range of variables used for the fit, the number of selected events, the selection efficiency and the background fractions for every decay channel are shown in Table 1.

Results

A common fit to all leptonic and semileptonic decay channels results in a simultaneous measurement of the Michel parameters ρ, η, ξ and $\xi\delta$, the chirality parameter ξ_h and the τ polarization $\mathcal{P}_\tau$. The measured single particle spectra are shown in Fig. 3 together with the result of the fit. As an example of the joint decay distributions, we show in Fig. 4 for the $\pi\rho$ final state the pion energy spectrum for different slices of the ω_ρ variable and vice versa for the ρ spectrum. At small values of ω_ρ, where τ^- with negative helicity are enriched, the pions from the τ^+ tend to be less energetic as expected for positive τ^+ helicity. With growing ω_ρ the pion spectrum becomes harder, showing clearly the spin correlations. The results of the measurement and the prediction of the Standard Model are summarized in Table 2. The χ^2 per degree of freedom resulting from the fit with statistical errors only is 1.16 with 2632 degrees of freedom. Correlation coefficients for the measured parameters are listed in Table 3.

We determine in an independent analysis the chirality parameter ξ_h and the τ polarization $\mathcal{P}_\tau$ from the final states $\pi\pi$, $\rho\rho$, $\rho\pi$, πX and ρX, where X means final states not identified as π or ρ. The h functions for this fit are constructed using Monte Carlo events passed through the full detector simulation, reconstruction and selection. The values obtained for $\mathcal{P}_\tau$ and ξ_h are $-0.165 \pm 0.017 \pm 0.011$ and $-0.960 \pm 0.051 \pm 0.012$, respectively, in agreement with the results above.

Systematic errors

Systematic errors are estimated for event selection, uncertainties in the background, the calibration of the subdetectors and Monte Carlo statistics. These sources are considered to be

Channel	Fit range		Events	ε (%) in 4π	Bkg. (%) τ	non-τ
e e	min x_e	$[0.05, 0.8]$	1005	34.4	2.0	3.1
	max x_e	$[0.15, 0.95]$				
e μ	x_e	$[0.05, 1.05]$	1322	26.1	1.9	0.5
	x_μ	$[0.05, 1.1]$				
e π	x_e	$[0.05, 1.05]$	1092	30.2	9.7	1.0
	x_π	$[0.09, 1.4]$				
e ρ	x_e	$[0.05, 1.]$	2269	30.0	13.5	0.2
	ω_ρ	$[-1., 1.]$				
e X	x_e	$[0.05, 1.1]$	5891	61.8	1.1	6.2
μ π	x_μ	$[0.05, 1.]$	802	25.2	10.8	5.6
	x_π	$[0.09, 1.4]$				
μ ρ	x_μ	$[0.05, 1.]$	1743	24.5	13.3	3.2
	ω_ρ	$[-1., 1.]$				
μ X	x_μ	$[0.05, 1.1]$	3870	42.5	0.6	5.6
π π	x_π	$[0.09, 1.4]$	371	26.3	15.3	2.5
π ρ	x_π	$[0.09, 1.4]$	1460	26.0	20.2	0.2
	ω_ρ	$[-1., 1.]$				
π X	x_π	$[0., 1.4]$	3733	57.0	10.3	2.3
ρ ρ	ω_ρ	$[-1., 1.]$	1624	25.7	24.0	0.2
ρ X	ω_ρ	$[-1., 1.]$	6830	52.5	13.0	0.4
Total			32012			

Table 1: The range of the variables used in the fit, the number of selected events, the selection efficiency and the background fractions from τ and non-τ background for each channel.

	this measurement	V$-$A prediction
ρ	$0.794 \pm 0.039 \pm 0.031$	0.75
η	$0.25 \pm 0.17 \pm 0.11$	0.
ξ	$0.94 \pm 0.21 \pm 0.07$	1.0
$\xi\delta$	$0.81 \pm 0.14 \pm 0.06$	0.75
ξ_h	$-0.970 \pm 0.053 \pm 0.011$	-1.0
$\mathcal{P}_\tau$	$-0.154 \pm 0.018 \pm 0.012$	

Table 2: The results for the Michel parameters, the chirality parameter ξ_h and the τ polarization $\mathcal{P}_\tau$ and their predictions in the Standard Model. The first error is statistical and the second systematic.

	η	ξ	$\xi\delta$	ξ_h	$\mathcal{P}_\tau$
ρ	0.455	−0.165	−0.279	−0.324	0.421
η		0.119	0.076	−0.010	0.020
ξ			0.033	0.106	0.144
$\xi\delta$				0.365	−0.262
ξ_h					−0.447

Table 3: The correlation coefficients for the Michel parameters, the chirality parameter and the τ polarization.

Uncertainty	$\Delta\,\rho$	$\Delta\,\eta$	$\Delta\,\xi$	$\Delta\,\xi\delta$	$\Delta\,\xi_h$	$\Delta\,\mathcal{P}_\tau$
selection	0.007	0.01	0.02	0.01	0.007	0.006
background	0.011	0.03	0.05	0.04	0.004	0.003
Calibration	0.026	0.08	0.04	0.03	0.006	0.009
MC statistics	0.012	0.06	0.02	0.04	0.003	0.005
Total	0.031	0.11	0.07	0.06	0.011	0.012

Table 4: Summary of the systematic errors on the τ polarization, the Michel parameters and the chirality parameter.

independent. The corresponding systematic errors have been estimated from the changes in the fitted values of the parameters, varying the cuts for the event selection, the fraction of background contamination and the energy calibrations of the subdetectors. Systematic errors due to event selection are small and mainly induced by cuts which correlate both hemispheres. The non-τ background is varied within the statistical error of its normalization. The uncertainties of the background from other τ decays are estimated by varying the branching ratios of τ decays within their errors [19]. They have a negligible effect on the results. The accuracy of the BGO energy scale is estimated from the π^0 peak position to be 1% at 1 GeV and from Bhabha events to be 0.1% at 45 GeV. The momentum scale of the central tracker is known within 1% from a comparison to muon momentum measurements in the muon spectrometer. The muon momentum scale is known to better than 0.2% at 45 GeV from dimuon events. At low momenta, the muon momentum uncertainty is dominated by energy losses in the calorimeters, which are known to an accuracy of 50 MeV. Possible energy scale errors for the BGO and HCAL for charged hadrons are estimated to be less than 1.5% from the peak position of the ρ resonance. The effect of finite Monte Carlo statistics is estimated by varying the acceptance values within their statistical errors. The summary of the systematic error study is given in Table 4.

Conclusion

A sample of 32012 $e^+e^- \to \tau^+\tau^-$ events collected by the L3 detector at LEP is selected with one or both τ decays identified as $\tau^- \to e^- \bar{\nu}_e \nu_\tau$, $\tau^- \to \mu^- \bar{\nu}_\mu \nu_\tau$, $\tau^- \to \pi^- \nu_\tau$ or $\tau^- \to \rho^- \nu_\tau$. Assuming only vector and axial vector couplings in the production process a measurement of the Michel parameters ρ, η, ξ and $\xi\delta$, the chirality parameter ξ_h and the average τ polarization $\mathcal{P}_\tau$ is performed. The results are summarized in Table 2. The results are comparable with

other recent measurements [5,6]. The value for the τ polarization $\mathcal{P}_\tau$ obtained in this analysis is in agreement with the result of our previous τ polarization measurement [18]. The values for all Michel parameters are in agreement with a V$-$A structure of the weak charged current interaction in τ lepton decays. The measurement of the chirality parameter ξ_h agrees with only left handed τ neutrinos in semileptonic τ decays.

Acknowledgements

The L3 Collaboration:

M.Acciarri[28] A.Adam[47] O.Adriani[17] M.Aguilar-Benitez[27] S.Ahlen[11] B.Alpat[35] J.Alcaraz[27] G.Alemanni[23]
J.Allaby[18] A.Aloisio[30] G.Alverson[12] M.G.Alviggi[30] G.Ambrosi[35] H.Anderhub[50] V.P.Andreev[39] T.Angelescu[13]
D.Antreasyan[9] A.Arefiev[29] T.Azemoon[3] T.Aziz[10] P.Bagnaia[38] L.Baksay[45] R.C.Ball[3] S.Banerjee[10] K.Banicz[47]
R.Barillère[18] L.Barone[38] P.Bartalini[35] A.Baschirotto[28] M.Basile[9] R.Battiston[35] A.Bay[23] F.Becattini[17] U.Becker[16]
F.Behner[50] J.Berdugo[27] P.Berges[16] B.Bertucci[18] B.L.Betev[50] M.Biasini[18] A.Biland[50] G.M.Bilei[35] J.J.Blaising[18]
S.C.Blyth[36] G.J.Bobbink[2] R.Bock[1] A.Böhm[1] B.Borgia[38] A.Boucham[4] D.Bourilkov[50] M.Bourquin[20] D.Boutigny[4]
E.Brambilla[16] J.G.Branson[41] V.Brigljevic[50] I.C.Brock[36] A.Buijs[46] A.Bujak[47] J.D.Burger[16] W.J.Burger[20]
J.Busenitz[45] A.Buytenhuijs[32] X.D.Cai[19] M.Campanelli[50] M.Capell[16] G.Cara Romeo[9] M.Caria[35] G.Carlino[4]
A.M.Cartacci[17] J.Casaus[27] G.Castellini[17] R.Castello[28] F.Cavallari[38] N.Cavallo[30] C.Cecchi[20] M.Cerrada[27]
F.Cesaroni[24] M.Chamizo[27] A.Chan[52] Y.H.Chang[52] U.K.Chaturvedi[19] M.Chemarin[26] A.Chen[52] G.Chen[7]
G.M.Chen[7] H.F.Chen[21] H.S.Chen[7] M.Chen[16] G.Chiefari[30] C.Y.Chien[5] M.T.Choi[44] L.Cifarelli[40] F.Cindolo[9]
C.Civinini[17] I.Clare[16] R.Clare[16] H.O.Cohn[33] G.Coignet[4] A.P.Colijn[2] N.Colino[27] V.Commichau[1] S.Costantini[38]
F.Cotorobai[13] B.de la Cruz[27] T.S.Dai[16] R.D'Alessandro[17] R.de Asmundis[30] H.De Boeck[32] A.Degré[4] K.Deiters[48]
P.Denes[37] F.DeNotaristefani[38] D.DiBitonto[45] M.Diemoz[38] D.van Dierendonck[2] F.Di Lodovico[50] C.Dionisi[38]
M.Dittmar[50] A.Dominguez[41] A.Doria[30] I.Dorne[4] M.T.Dova[19,♮] E.Drago[30] D.Duchesneau[4] P.Duinker[2] I.Duran[42]
S.Dutta[10] S.Easo[35] Yu.Efremenko[33] H.El Mamouni[26] A.Engler[36] F.J.Eppling[16] F.C.Erné[2] J.P.Ernenwein[26]
P.Extermann[20] M.Fabre[48] R.Faccini[38] S.Falciano[38] A.Favara[17] J.Fay[26] M.Felcini[50] C.Furetta[28] T.Ferguson[36]
D.Fernandez[27] F.Ferroni[38] H.Fesefeldt[1] E.Fiandrini[35] J.H.Field[20] F.Filthaut[36] P.H.Fisher[16] G.Forconi[16] L.Fredj[20]
K.Freudenreich[50] Yu.Galaktionov[29,16] S.N.Ganguli[10] S.S.Gau[12] S.Gentile[38] J.Gerald[5] N.Gheordanescu[13]
S.Giagu[38] S.Goldfarb[23] J.Goldstein[11] Z.F.Gong[21] A.Gougas[5] G.Gratta[34] M.W.Gruenewald[8] V.K.Gupta[37]
A.Gurtu[10] L.J.Gutay[47] K.Hangarter[1] B.Hartmann[1] A.Hasan[31] T.Hebbeker[8] A.Hervé[18] W.C.van Hoek[32]
H.Hofer[50] H.Hoorani[20] S.R.Hou[52] G.Hu[19] M.M.Ilyas[19] V.Innocente[18] H.Janssen[4] B.N.Jin[7] L.W.Jones[3]
P.de Jong[16] I.Josa-Mutuberria[27] A.Kasser[23] R.A.Khan[19] Yu.Kamyshkov[33] P.Kapinos[49] J.S.Kapustinsky[25]
Y.Karyotakis[4] M.Kaur[19,◇] M.N.Kienzle-Focacci[20] D.Kim[5] J.K.Kim[44] S.C.Kim[44] Y.G.Kim[44] W.W.Kinnison[25]
A.Kirkby[34] D.Kirkby[34] J.Kirkby[18] W.Kittel[32] A.Klimentov[16,29] A.C.König[32] A.Köngeter[1] I.Korolko[29]
V.Koutsenko[16,29] A.Koulbardis[39] R.W.Kraemer[36] T.Kramer[16] W.Krenz[1] H.Kuijten[32] A.Kunin[16,29]
P.Ladron de Guevara[27] G.Landi[17] C.Lapoint[16] K.Lassila-Perini[50] M.Lebeau[18] A.Lebedev[16] P.Lebrun[26]
P.Lecomte[50] P.Lecoq[18] P.Le Coultre[50] J.S.Lee[44] K.Y.Lee[44] C.Leggett[3] J.M.Le Goff[18] R.Leiste[49] M.Lenti[17]
E.Leonardi[38] P.Levtchenko[39] C.Li[21] E.Lieb[49] W.T.Lin[52] F.L.Linde[2,18] B.Lindemann[1] L.Lista[30] Z.A.Liu[7]
W.Lohmann[49] E.Longo[38] W.Lu[34] Y.S.Lu[7] K.Lübelsmeyer[1] C.Luci[38] D.Luckey[16] L.Ludovici[38] L.Luminari[38]
W.Lustermann[48] W.G.Ma[21] A.Macchiolo[17] M.Maity[10] G.Majumder[10] L.Malgeri[38] A.Malinin[29] C.Maña[27]
S.Mangla[10] P.Marchesini[50] A.Marin[11] J.P.Martin[26] F.Marzano[38] G.G.G.Massaro[2] K.Mazumdar[10] D.McNally[18]
S.Mele[30] L.Merola[30] M.Meschini[17] W.J.Metzger[32] M.von der Mey[1] Y.Mi[23] A.Mihul[13] A.J.W.van Mil[32]
G.Mirabelli[38] J.Mnich[18] M.Möller[1] B.Monteleoni[17] R.Moore[3] S.Morganti[38] R.Mount[34] S.Müller[1] F.Muheim[20]
E.Nagy[14] S.Nahn[16] M.Napolitano[30] F.Nessi-Tedaldi[50] H.Newman[34] A.Nippe[1] H.Nowak[49] G.Organtini[38]
R.Ostonen[22] D.Pandoulas[1] S.Paoletti[38] P.Paolucci[30] H.K.Park[36] G.Pascale[38] G.Passaleva[17] S.Patricelli[30]
T.Paul[35] M.Pauluzzi[35] C.Paus[1] F.Pauss[50] D.Peach[18] Y.J.Pei[1] S.Pensotti[28] D.Perret-Gallix[4] S.Petrak[8]
A.Pevsner[5] D.Piccolo[30] M.Pieri[17] J.C.Pinto[36] P.A.Piroué[37] E.Pistolesi[17] V.Plyaskin[29] M.Pohl[50] V.Pojidaev[29,17]
H.Postema[16] N.Produit[20] R.Raghavan[10] G.Rahal-Callot[50] P.G.Rancoita[28] M.Rattaggi[28] G.Raven[41]
P.Razis[31] K.Read[33] D.Ren[50] M.Rescigno[38] S.Reucroft[12] T.van Rhee[46] A.Ricker[1] S.Riemann[49] B.C.Riemers[47]
K.Riles[3] O.Rind[3] S.Ro[44] A.Robohm[50] J.Rodin[16] F.J.Rodriguez[27] B.P.Roe[3] S.Röhner[1] L.Romero[27]
S.Rosier-Lees[4] Ph.Rosselet[23] W.van Rossum[46] S.Roth[1] J.A.Rubio[18] H.Rykaczewski[50] J.Salicio[18] E.Sanchez[27]
A.Santocchia[35] M.E.Sarakinos[22] S.Sarkar[10] M.Sassowsky[1] G.Sauvage[4] C.Schäfer[1] V.Schegelsky[39]
S.Schmidt-Kaerst[1] D.Schmitz[1] P.Schmitz[1] M.Schneegans[4] B.Schoeneich[49] N.Scholz[50] H.Schopper[51]
D.J.Schotanus[32] R.Schulte[1] K.Schultze[1] J.Schwenke[1] G.Schwering[1] C.Sciacca[30] D.Sciarrino[20] J.C.Sens[52]
L.Servoli[35] S.Shevchenko[34] N.Shivarov[43] V.Shoutko[29] J.Shukla[25] E.Shumilov[29] T.Siedenburg[1] D.Son[44]
A.Sopczak[49] V.Soulimov[30] B.Smith[16] P.Spillantini[17] M.Steuer[16] D.P.Stickland[37] F.Sticozzi[16] H.Stone[37]
B.Stoyanov[43] A.Straessner[1] K.Strauch[15] K.Sudhakar[10] G.Sultanov[19] L.Z.Sun[21] G.F.Susinno[20] H.Suter[50]
J.D.Swain[19] X.W.Tang[7] L.Tauscher[6] L.Taylor[12] Samuel C.C.Ting[16] S.M.Ting[16] O.Toker[35] F.Tonisch[49]
M.Tonutti[1] S.C.Tonwar[10] J.Tóth[14] A.Tsaregorodtsev[39] C.Tully[37] H.Tuchscherer[45] K.L.Tung[7] J.Ulbricht[50]
U.Uwer[18] E.Valente[38] R.T.Van de Walle[32] I.Vetlitsky[29] G.Viertel[50] M.Vivargent[4] R.Völkert[49] H.Vogel[36]
H.Vogt[49] I.Vorobiev[29] A.A.Vorobyov[39] An.A.Vorobyov[39] A.Vorvolakos[31] M.Wadhwa[6] W.Wallraff[1] J.C.Wang[16]
X.L.Wang[21] Y.F.Wang[16] Z.M.Wang[21] A.Weber[1] F.Wittgenstein[18] S.X.Wu[19] S.Wynhoff[1] J.Xu[11] Z.Z.Xu[21]
B.Z.Yang[21] C.G.Yang[7] X.Y.Yao[7] J.B.Ye[21] S.C.Yeh[52] J.M.You[36] C.Zaccardelli[34] An.Zalite[39] P.Zemp[50] Y.Zeng[1]
Z.Zhang[7] Z.P.Zhang[21] B.Zhou[11] Y.Zhou[3] G.Y.Zhu[7] R.Y.Zhu[34] A.Zichichi[9,18,19]

1 I. Physikalisches Institut, RWTH, D-52056 Aachen, FRG[§]
   III. Physikalisches Institut, RWTH, D-52056 Aachen, FRG[§]
2 National Institute for High Energy Physics, NIKHEF, and University of Amsterdam, NL-1009 DB Amsterdam, The Netherlands
3 University of Michigan, Ann Arbor, MI 48109, USA
4 Laboratoire d'Annecy-le-Vieux de Physique des Particules, LAPP,IN2P3-CNRS, BP 110, F-74941 Annecy-le-Vieux CEDEX, France
5 Johns Hopkins University, Baltimore, MD 21218, USA
6 Institute of Physics, University of Basel, CH-4056 Basel, Switzerland
7 Institute of High Energy Physics, IHEP, 100039 Beijing, China
8 Humboldt University, D-10099 Berlin, FRG[§]
9 INFN-Sezione di Bologna, I-40126 Bologna, Italy
10 Tata Institute of Fundamental Research, Bombay 400 005, India
11 Boston University, Boston, MA 02215, USA
12 Northeastern University, Boston, MA 02115, USA
13 Institute of Atomic Physics and University of Bucharest, R-76900 Bucharest, Romania
14 Central Research Institute for Physics of the Hungarian Academy of Sciences, H-1525 Budapest 114, Hungary[‡]
15 Harvard University, Cambridge, MA 02139, USA
16 Massachusetts Institute of Technology, Cambridge, MA 02139, USA
17 INFN Sezione di Firenze and University of Florence, I-50125 Florence, Italy
18 European Laboratory for Particle Physics, CERN, CH-1211 Geneva 23, Switzerland
19 World Laboratory, FBLJA Project, CH-1211 Geneva 23, Switzerland
20 University of Geneva, CH-1211 Geneva 4, Switzerland
21 Chinese University of Science and Technology, USTC, Hefei, Anhui 230 029, China
22 SEFT, Research Institute for High Energy Physics, P.O. Box 9, SF-00014 Helsinki, Finland
23 University of Lausanne, CH-1015 Lausanne, Switzerland
24 INFN-Sezione di Lecce and Universitá Degli Studi di Lecce, I-73100 Lecce, Italy
25 Los Alamos National Laboratory, Los Alamos, NM 87544, USA
26 Institut de Physique Nucléaire de Lyon, IN2P3-CNRS,Université Claude Bernard, F-69622 Villeurbanne, France
27 Centro de Investigaciones Energeticas, Medioambientales y Tecnologicas, CIEMAT, E-28040 Madrid, Spain[♭]
28 INFN-Sezione di Milano, I-20133 Milan, Italy
29 Institute of Theoretical and Experimental Physics, ITEP, Moscow, Russia
30 INFN-Sezione di Napoli and University of Naples, I-80125 Naples, Italy
31 Department of Natural Sciences, University of Cyprus, Nicosia, Cyprus
32 University of Nymegen and NIKHEF, NL-6525 ED Nymegen, The Netherlands
33 Oak Ridge National Laboratory, Oak Ridge, TN 37831, USA
34 California Institute of Technology, Pasadena, CA 91125, USA
35 INFN-Sezione di Perugia and Universitá Degli Studi di Perugia, I-06100 Perugia, Italy
36 Carnegie Mellon University, Pittsburgh, PA 15213, USA
37 Princeton University, Princeton, NJ 08544, USA
38 INFN-Sezione di Roma and University of Rome, "La Sapienza", I-00185 Rome, Italy
39 Nuclear Physics Institute, St. Petersburg, Russia
40 University and INFN, Salerno, I-84100 Salerno, Italy
41 University of California, San Diego, CA 92093, USA
42 Dept. de Fisica de Particulas Elementales, Univ. de Santiago, E-15706 Santiago de Compostela, Spain
43 Bulgarian Academy of Sciences, Central Laboratory of Mechatronics and Instrumentation, BU-1113 Sofia, Bulgaria
44 Center for High Energy Physics, Korea Advanced Inst. of Sciences and Technology, 305-701 Taejon, Republic of Korea
45 University of Alabama, Tuscaloosa, AL 35486, USA
46 Utrecht University and NIKHEF, NL-3584 CB Utrecht, The Netherlands
47 Purdue University, West Lafayette, IN 47907, USA
48 Paul Scherrer Institut, PSI, CH-5232 Villigen, Switzerland
49 DESY-Institut für Hochenergiephysik, D-15738 Zeuthen, FRG
50 Eidgenössische Technische Hochschule, ETH Zürich, CH-8093 Zürich, Switzerland
51 University of Hamburg, D-22761 Hamburg, FRG
52 High Energy Physics Group, Taiwan, China
§ Supported by the German Bundesministerium für Bildung, Wissenschaft, Forschung und Technologie
‡ Supported by the Hungarian OTKA fund under contract number T14459.
♭ Supported also by the Comisión Interministerial de Ciencia y Technología
♯ Also supported by CONICET and Universidad Nacional de La Plata, CC 67, 1900 La Plata, Argentina
◇ Also supported by Panjab University, Chandigarh-160014, India

References

[1] L. Michel, Proc. Phys. Soc. **A 63** (1950) 514;
C. Bouchiat and L. Michel, Phys. Rev. **106** (1957) 170;
T. Kinoshita and A. Sirlin, Phys. Rev. **107** (1957) 593;
T. Kinoshita and A. Sirlin, Phys. Rev. **108** (1957) 844.

[2] W. Fetscher, H. J. Gerber and K. F. Johnson, Phys. Lett. **B 173** (1986) 102.

[3] B. Balke *et al.*, Phys. Rev. **D 37** (1988) 587.

[4] DELCO Collab., W. Bacino *et al.*, Phys. Rev. Lett. **42** (1979) 749;
CLEO Collab., S. Behrends *et al.*, Phys. Rev. **D 32** (1985) 2468;
MAC Collab., W. T. Ford *et al.*, Phys. Rev. **D 36** (1987) 1971;
CBAL Collab., H. Janssen *et al.*, Phys. Lett. **B 228** (1989) 273;
ARGUS Collab., H. Albrecht *et al.*, Phys. Lett. **B 316** (1993) 608.

[5] ARGUS Collab., H. Albrecht *et al.*, Phys. Lett. **B 341** (1995) 441;
ARGUS Collab., H. Albrecht *et al.*, Phys. Lett. **B 349** (1995) 576.

[6] ALEPH Collab., D. Busculic *et al.*, Phys. Lett. **B 346** (1995) 379.

[7] F. Scheck, Leptons, Hadrons and Nuclei, North Holland Physics Publishing, Amsterdam (1983).

[8] K. Mursula and F. Scheck, Nucl. Phys. **B 253** (1985) 189.

[9] C. Nelson, Phys. Rev. **D 40** (1989) 123, erratum Phys. Rev. **D 41** (1990) 2327;
W. Fetscher, Phys. Rev. **D 42** (1990) 1544;
R. Alemany *et al.*, Nucl. Phys. **B 379** (1992) 3.

[10] M. Davier, L. Duflot, F. Le Diberder and A. Rougé, Phys. Lett. **B 306** (1993) 411.

[11] SLD Collab., K. Abe *et al.*, Phys. Rev. Lett. **70** (1993) 2515.

[12] ARGUS Collab., H. Albrecht *et al.*, Phys. Lett. **B250** (1990) 164.

[13] L3 Collab., B. Adeva *et al.*, Nucl. Inst. and Meth. **A 289** (1990) 35.

[14] L3 Collab., O. Adriani *et al.*, Phys. Lett. **B 294** (1992) 466.

[15] S. Jadach, B.F.L. Ward and Z. Wąs, Comp. Phys. Comm. **66** (1991) 276.

[16] M. Schmidtler, "A Convenient Parametrization for the General Matrix Element of Leptonic Tau Decay", Preprint IEKP-KA/93-14, University Karlsruhe, (Karlsruhe 1993).

[17] S. Jadach, Z. Was *et al.*, in "Z Physics at LEP 1", CERN Report CERN 89-08, eds G. Altarelli, R. Kleiss and C. Verzegnassi (CERN, Geneva, 1989) Vol. 1, p. 235 and references therein..

[18] L3 Collab., M. Acciarri *et al.*, Phys. Lett. **B 341** (1994) 245.
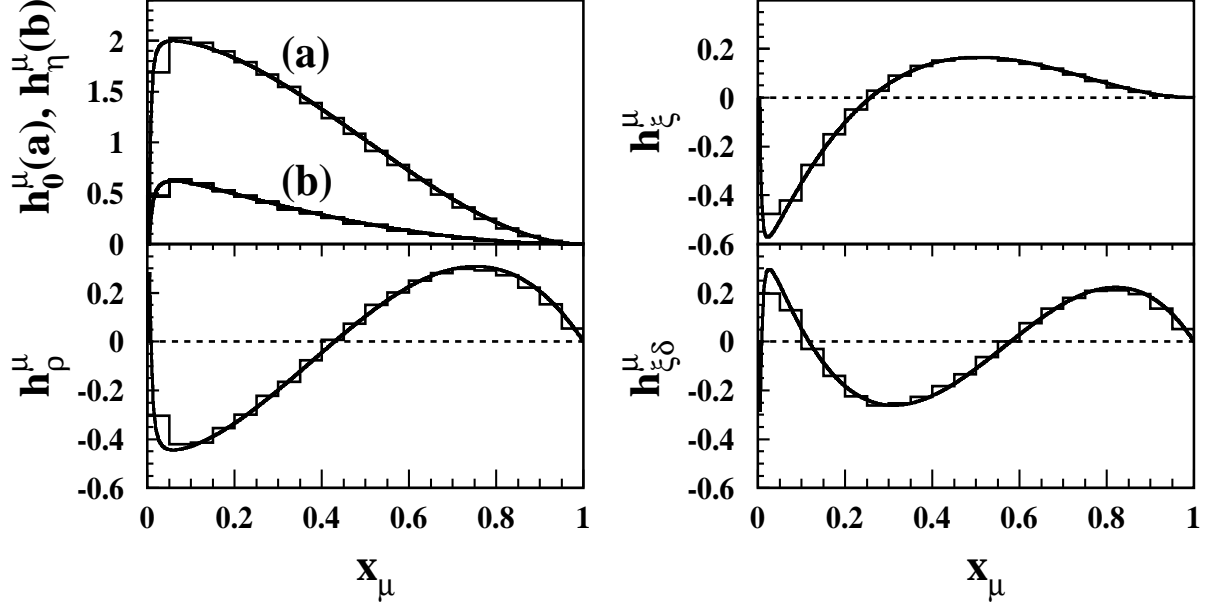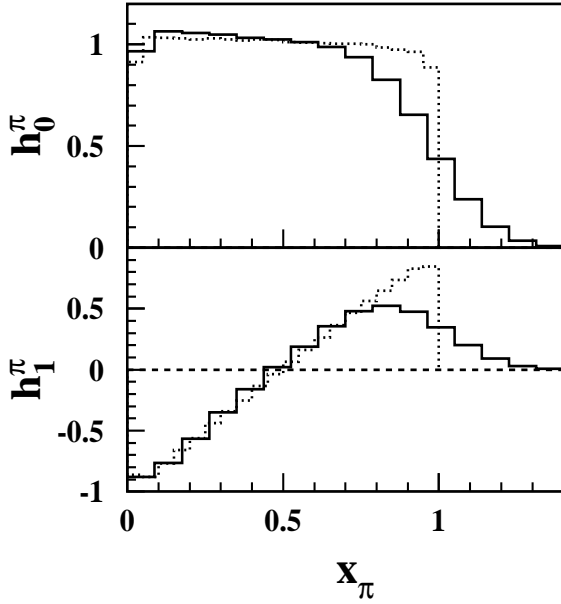
[19] Particle Data Group, Phys. Rev. **D 50** (1994) 1173.

$\tau \rightarrow \mu\nu\nu$

Figure 1: The functions $h_0(x), h_\rho(x), h_\eta(x), h_\xi(x)$ and $h_{\xi\delta}(x)$ for the $\tau^- \rightarrow \mu^- \bar{\nu}_\mu \nu_\tau$ decay. The solid lines are Born level calculations and the histograms result from the KORALZ Monte Carlo generator [15] including radiative corrections.
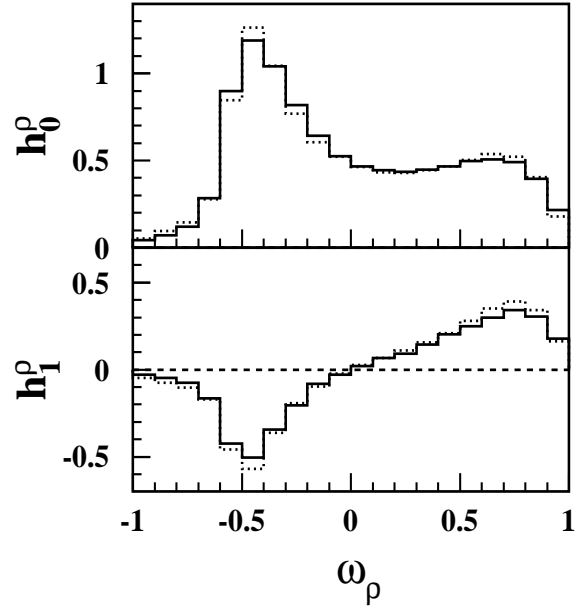
$\tau \rightarrow \pi\nu$ $\tau \rightarrow \rho\nu$

Figure 2: The functions $h_0(x)$ and $h_1(x)$ for the decays $\tau^- \rightarrow \pi^- \nu_\tau$ and $\tau^- \rightarrow \rho^- \nu_\tau$. The dashed lines correspond to the distributions obtained from the KORALZ Monte Carlo generator [15]. The solid lines include the effects of detector resolution functions and acceptances.
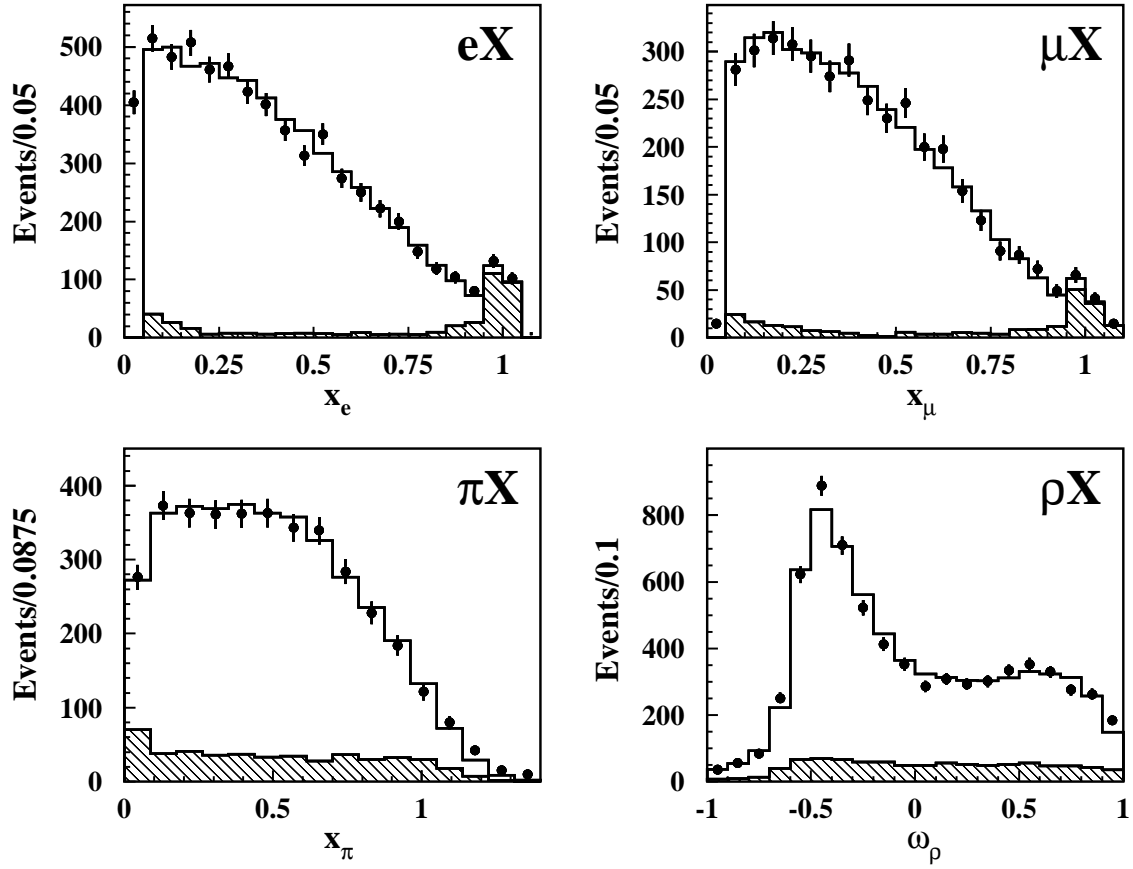
Figure 3: Observed spectra from eX, μX, πX and ρX final states (dots) with results of the fit (solid histogram) superimposed. The sum of τ and non-τ background is shown as hatched histograms.
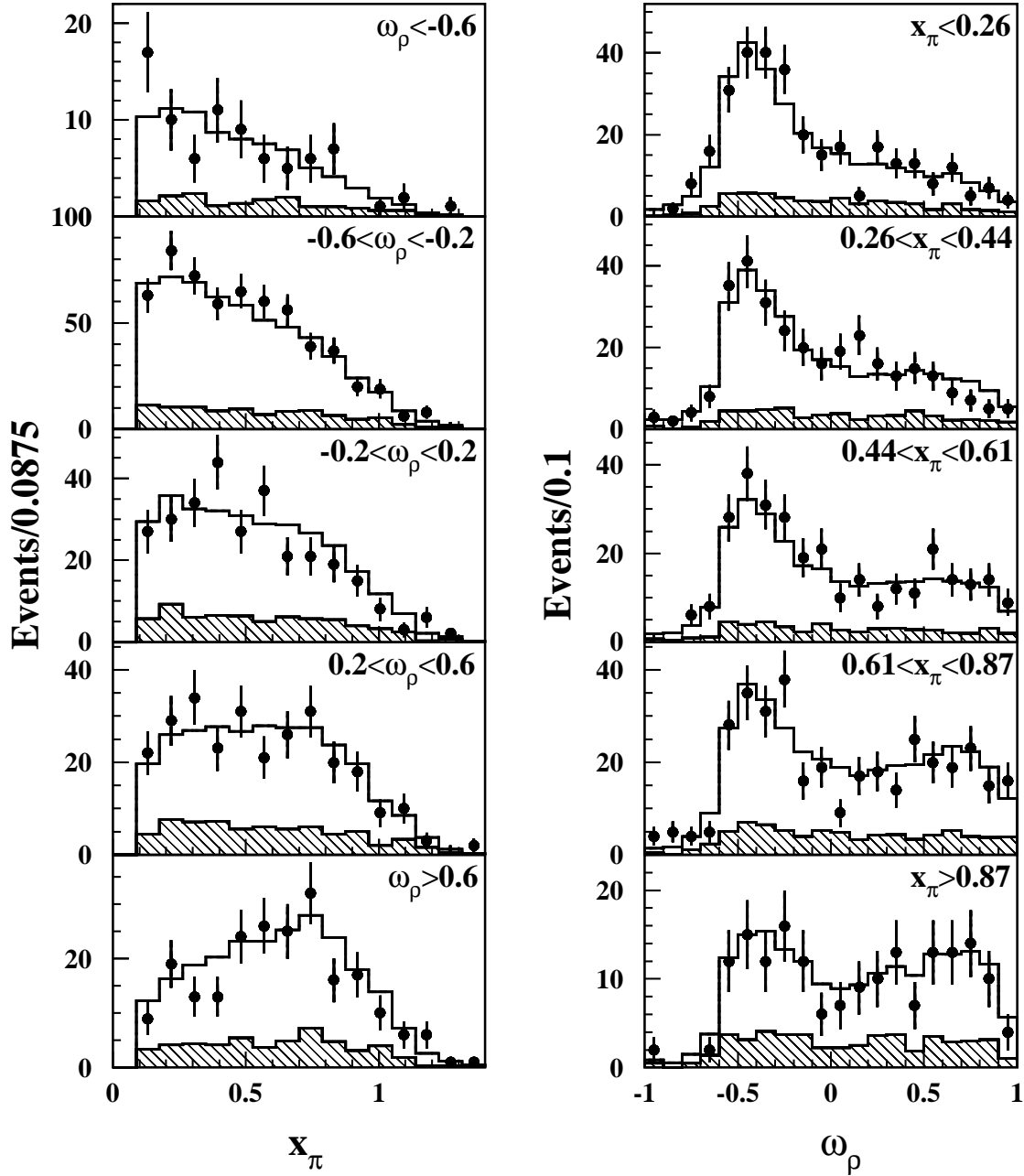
Figure 4: The π and ρ spectra from $e^+e^- \rightarrow \tau^+\tau^- \rightarrow \pi^\pm \rho^\mp \nu_\tau \bar{\nu}_\tau$. On the left side the normalized pion energy spectrum is shown for different slices of the ω_ρ variable. On the right side ω_ρ is shown for different slices of the normalized pion energy. The results of the fit (solid histogram) are superimposed. The sum of τ and non-τ background is shown as hatched histograms.